

Supporting Information

In Situ Quantification of Surface Intermediates and Correlation to Discharge Products on Hematite Photoanodes using a Combined Scanning Electrochemical Microscopy Approach

Mihail R. Krumov,^{&,\ddagger} Burton H Simpson,^{&,\ddagger,\dagger} Michael J. Coughlan[&], Joaquín Rodríguez-López^{&,\#,*}

[&] Department of Chemistry, University of Illinois at Urbana-Champaign, 600 South Mathews Avenue, Urbana, IL 61801 *Corresponding author e-mail: joaquinr@illinois.edu; Phone: +1 (217) 300-7354.

[#] Beckman Institute for Advanced Science and Technology, University of Illinois at Urbana-Champaign

TABLE OF CONTENTS

S1. Numerical Simulations

Table S1. Atomic percents of species in the hematite samples as calculated from XPS measurements

Figure S1. Schematic of COMSOL model

Figure S2. Cross sectional SEM of Ti-Fe₂O₃ sample

Figure S3. XPS survey spectrum of Ti-Fe₂O₃ sample

Figure S4. GI-XRD diffractogram of Ti-Fe₂O₃ sample

Figure S5. Comparison of diffractogram to standard materials

Figure S6. Comparison of FTO and Ti-Fe₂O₃ diffractograms

Figure S7. IPCE measurement of Ti-Fe₂O₃ sample

Figure S8. LSVs of Ti-Fe₂O₃ sample under different illuminations conditions

Figure S9. SI-SECM under visible illumination

Figure S10. SI-SECM with delay times

Figure S11. Cyclic voltammetry of carbon microelectrode

Figure S12. Approach curve of carbon microelectrode

Figure S13. Calibration of platinum microelectrode response to hydrogen peroxide

S1 Numerical Simulations

Numerical simulation of the combined diffusion and kinetic behaviors relies on three key assumptions, as described in an earlier publication describing our simulations framework.¹ First, we assume that all chemical transport in the mediator solution is due to diffusion described by Fick's first and second laws, as shown in Figure S.1. Second, we assume that the adsorbed species is immobile and that lateral charge transfer is insignificant. Third, we assume the rate constants k_{si1} and k_{si2} for the bimolecular reactions of the first and second adsorbed species, respectively, with the mediator is assumed to be constant regardless of surface coverage.

Figure 2 shows a schematic of the geometry used for the simulations of SI-SECM. Using the Transport of Dilute Species Module (TDSM), the COMSOL model employed Fick's First and Second laws to simulate diffusion in the domains corresponding to the solution phase, represented as yellow areas in Fig. 2. Type 1 boundaries are the insulating glass sheath of the electrode, where the No Flux condition was used. The Type 2 boundary uses a Flux boundary condition that mimics fast Butler-Volmer kinetics $i = k_f c_R - k_b c_O$ with an effectively high k_f such that it always operates at mass transfer limited conditions. The diffusion coefficient of O and R was made equal, such that stoichiometry between O and R is maintained at all points in the solution space. At Type 3 boundaries, the Surface Reactions Module (SRM) is used to define a surface containing the adsorbed species $I_{(ads)j}$. The bimolecular reaction of $I_{(ads)j}$ with O is modeled as a Reaction in the SRM and an Inward Flux in the TDSM, each with the equation $N_O = -N_R = -R_{A,j} = k_{si,j} c_R T_A$, where subscript j indicates the assigned number of the adsorbed species. Sections S1, S2, and S3 were defined as the substrate areas below the UME, the glass sheath of the tip, and open solution, respectively, as these distinctions facilitate later discussion. To meet the semi-infinite diffusion conditions of the electrochemical cell, Type 4 boundaries used a concentration boundary condition that set both R and O to their initial conditions.

The SI-SECM transient tip current (i_{tip}) was measured by integrating the diffusive flux of R to the Type 1 boundary. The simulated surface interrogation current (i_{si}) was calculated by subtracting $i_{tip}(I_A = 0)$ from a simulated transient. The resulting titrated charge, Q_{si} , was obtained by integrating i_{si} with respect to time, but here, we frequently normalized by the steady-state limiting current to give $I_{si} = i_{si}/i_{ss}$. Q_{si} was normalized by the charge present on the area of the tip projected onto the substrate, Q_{proj} , i.e. the charge corresponding to a substrate of the same size of the tip micro-disk with radius a . This was done to demonstrate impact of diffusional broadening on Q_{si} , and this is referred to as the enhancement factor (EF). Expected positive (i_{PF}) and negative (i_{NF}) feedback currents for simulated conditions were calculated using reported general solutions for feedback accurate to approximately 1% across a wide range of conditions.²

Table S1: Atomic percents of species in the hematite samples as calculated from XPS measurements

Hematite 1				
Peak	% Conc in atom region	% Conc in total sample	% At. conc	Fe:Ti At. ratio
Fe2p_{1/2} (Fe³⁺) sat.	5.38	1.14	35.11	5.05
Fe2p_{1/2}	27.65	9.04		
Fe³⁺	3.27	0.43		
Fe2p_{3/2}	63.70	24.5	57.93	
O1s	100	57.93		
Ti2p_{1/2}	32.38	1.54	6.95	
Ti2p_{3/2}	67.62	5.41		

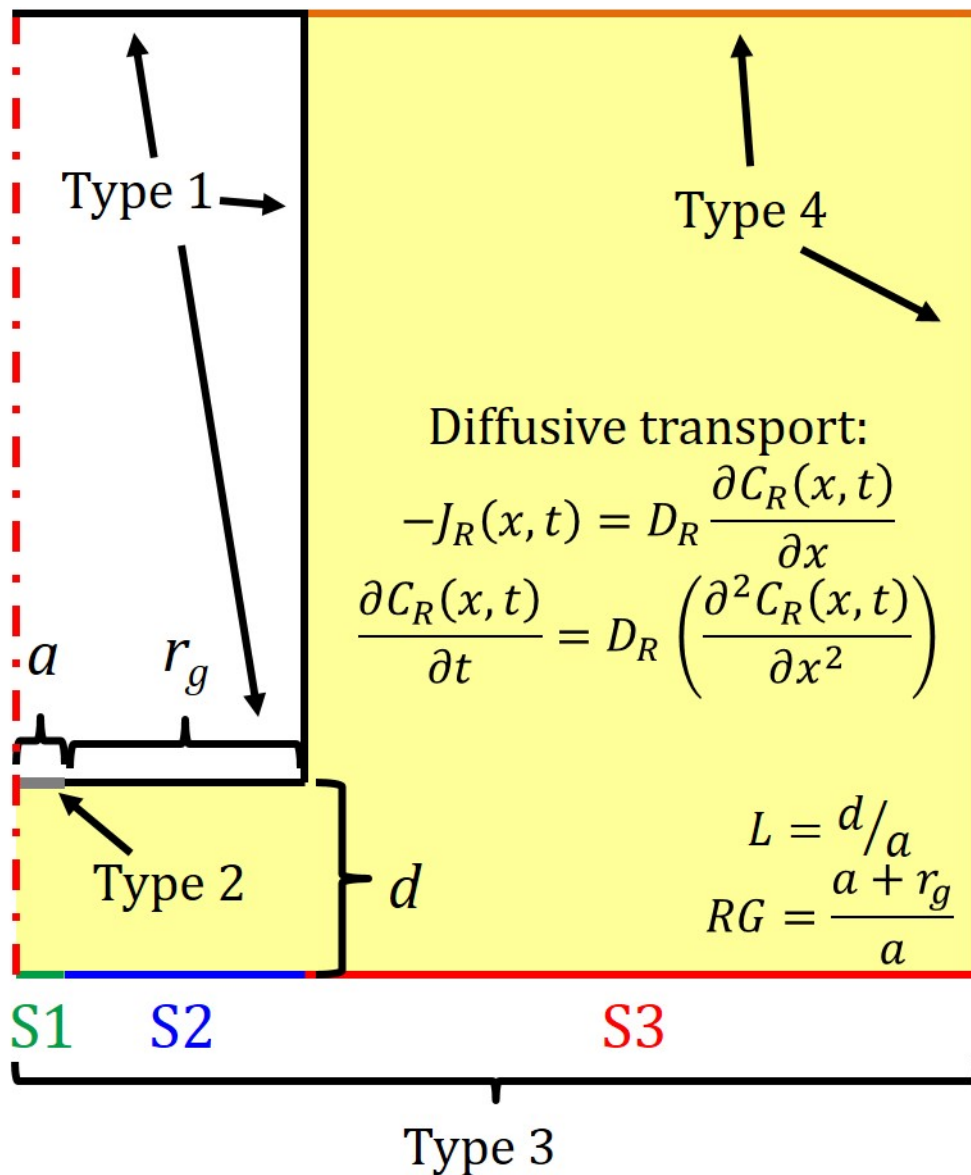


Figure S1. A radial cross-section of the 2D axis-symmetric COMSOL model used to simulate surface interrogations. Type 1, 2, and 4 boundaries simulate insulating surfaces, the UME tip, and semi-infinite diffusion within TDSM domains represented by the yellow domains. Type 3 boundaries use the TDSM and SRM to simulate bimolecular reactions occurring at a surface. Reprinted from *Electrochimica Acta*, 179 B. H. Simpson and J. Rodriguez-Lopez, Redox Titrations via Surface Interrogation Scanning Electrochemical Microscopy at an Extended Semiconducting Surface for the Quantification of Photogenerated Adsorbed Intermediates, 74-83. Copyright 2015, with permission from Elsevier.

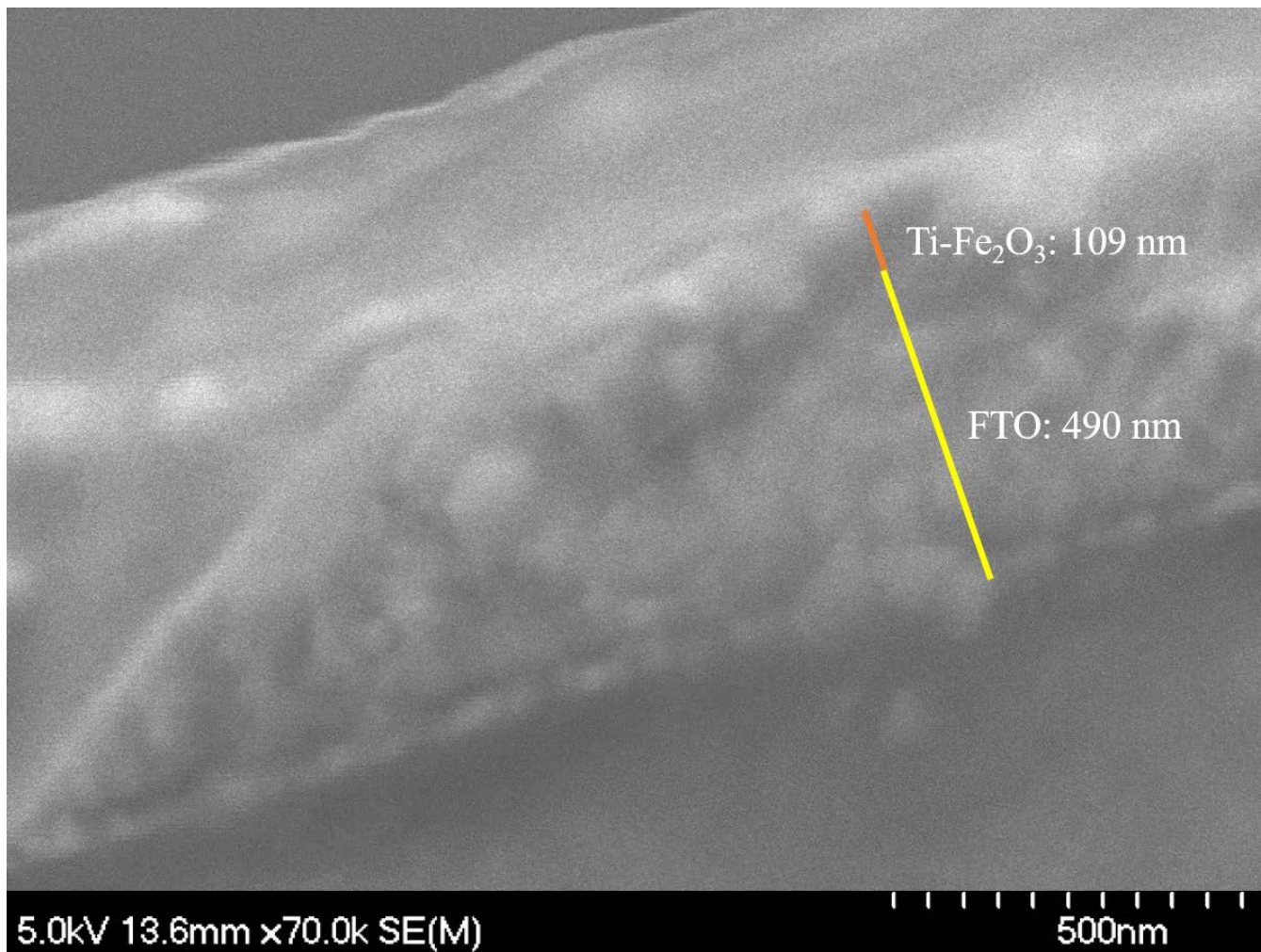


Figure S2. Cross-sectional SEM of the hematite sample showing the thickness of the deposited Ti-Fe₂O₃ is ~110 nm.

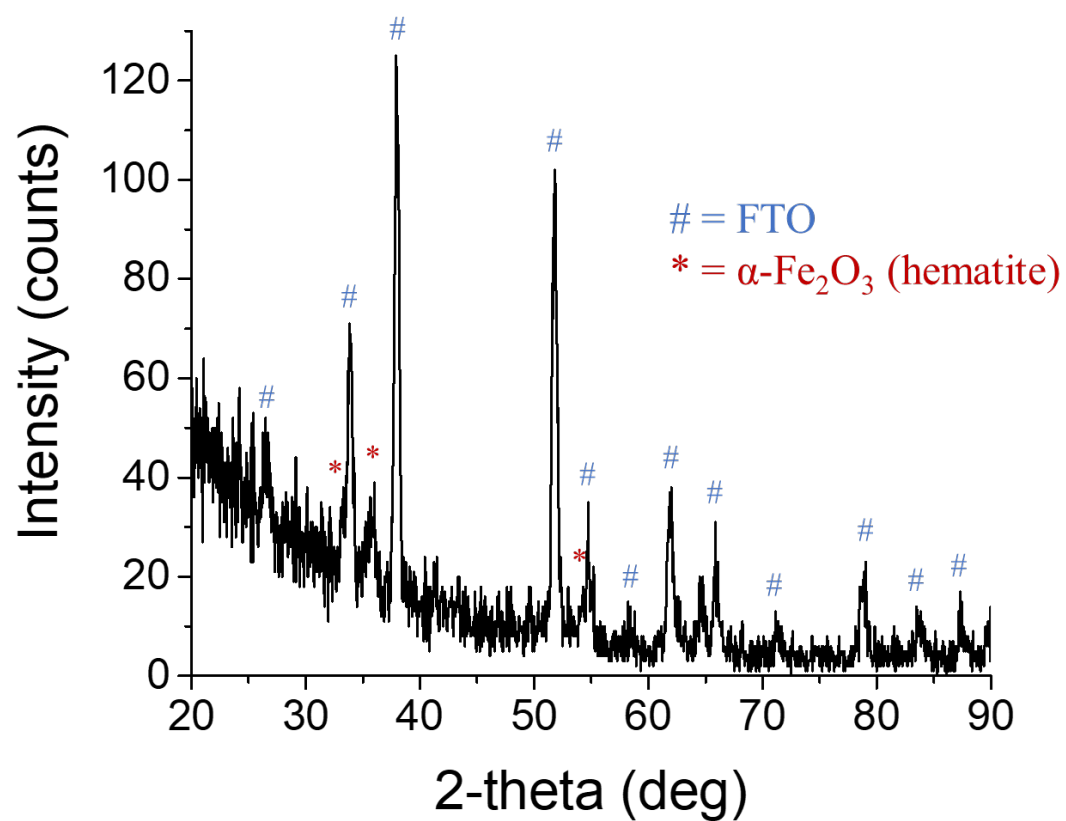


Figure S4. GI-XRD diffractogram of hematite sample 1 on FTO glass. Data were obtained with Cu-K α radiation source (45 kV tension, 40 mA current), Ni filter, beam size of 1 x 5 mm, grazing angle of 1.0°, step size of 0.05°, 0.5 s/step.

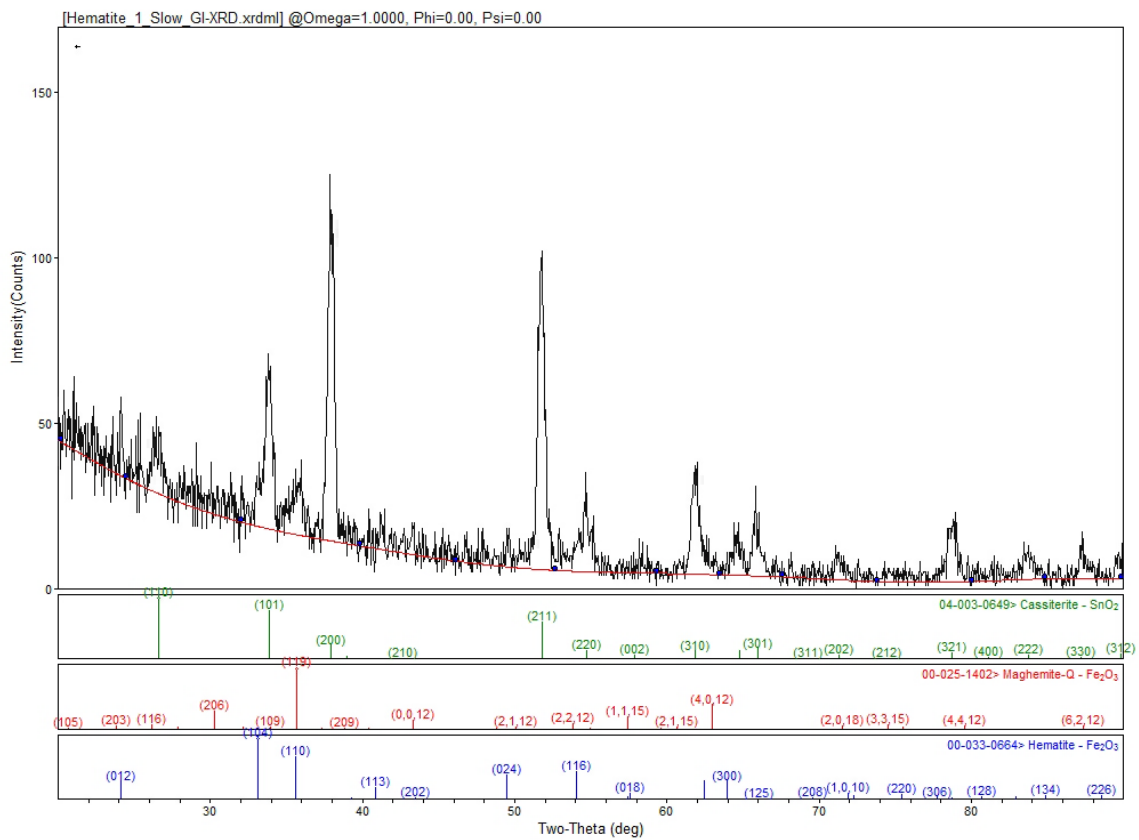


Figure S5. Comparison of acquired hematite diffractogram to reference peaks for SnO₂, hematite (α -Fe₂O₃), and maghemite (Fe₂O₃).

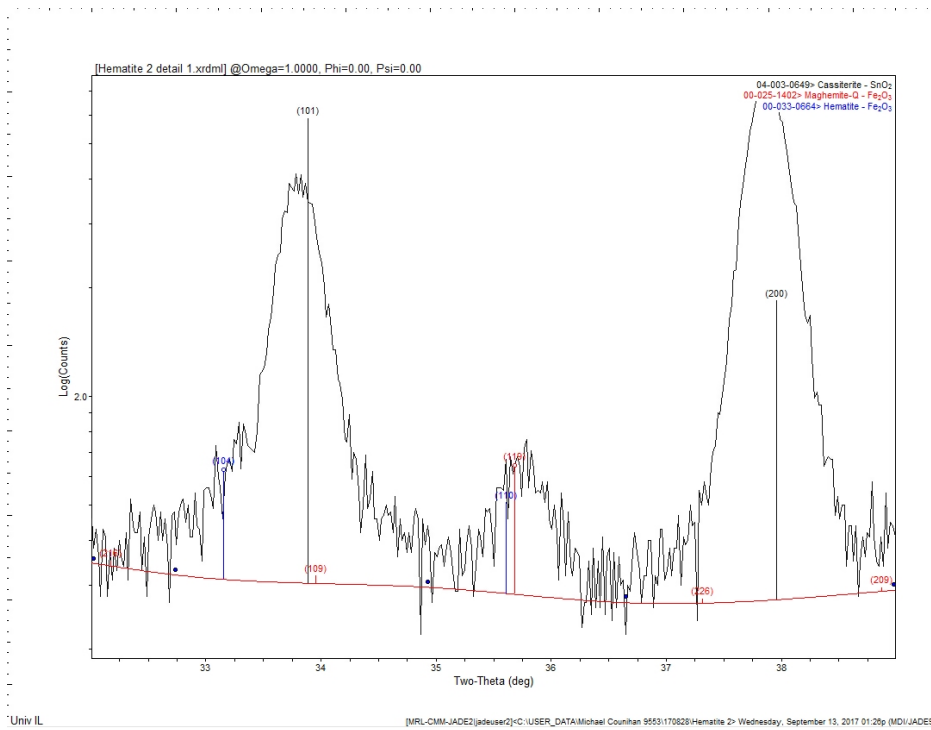
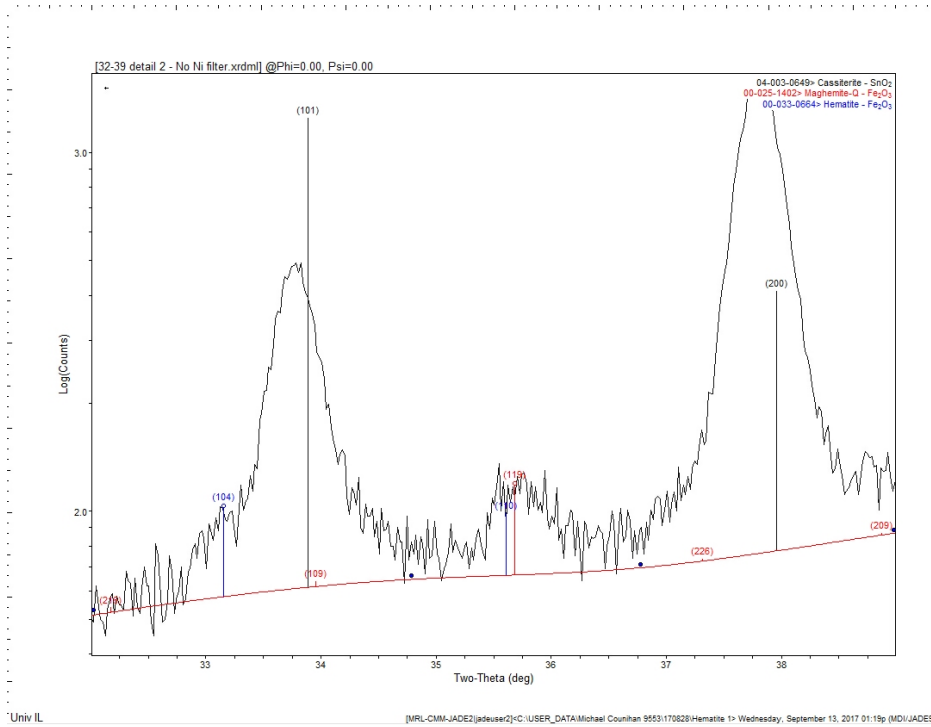


Figure S6. Detailed GI-XRD scan and reference comparison of hematite 1 (top) and hematite 2 (bottom) on FTO glass. Data were obtained with Cu-K α radiation source (45 kV tension, 40 mA current), Ni filter, beam size of 1 x 5 mm, grazing angle of 1.0°, step size of 0.02°, 4 s/step.

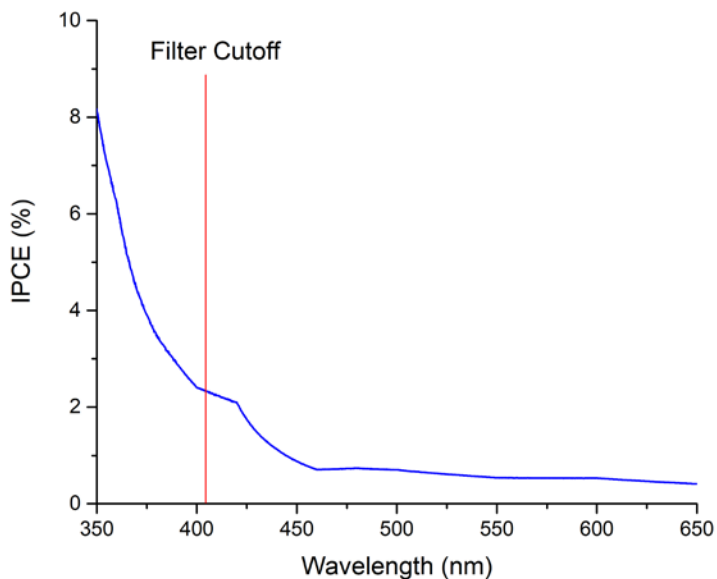


Figure S7. IPCE as a function of wavelength for the Ti-doped Hematite sample. The vertical line indicates the cutoff wavelength, 405 nm, of the light filter used to for visible illumination experiments. The integrated areas of visible and broadband illumination are 1.91 and 4.24 nm respectively. Recorded in 0.1 M NaOH.

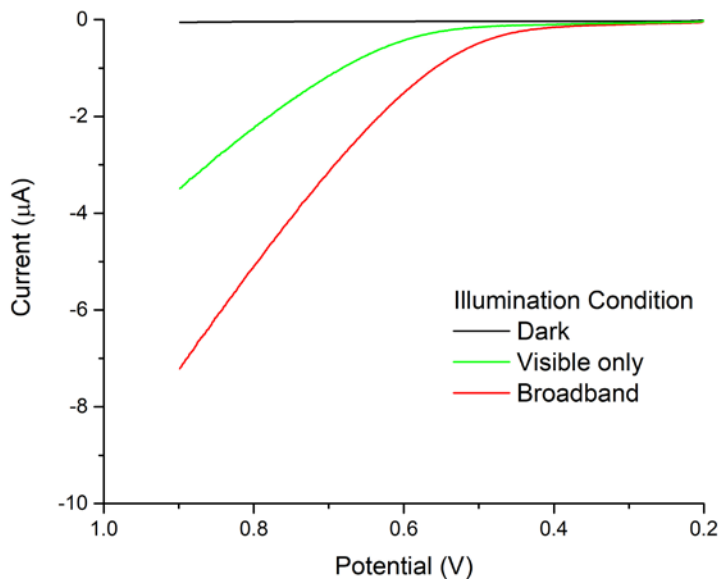


Figure S8. Steady state water oxidation current as a function of activation potential measured on Ti-doped hematite electrodes under different illumination conditions. The linear sweep voltammograms were recorded at a scan rate of 20 mV/s in 0.1 M NaOH

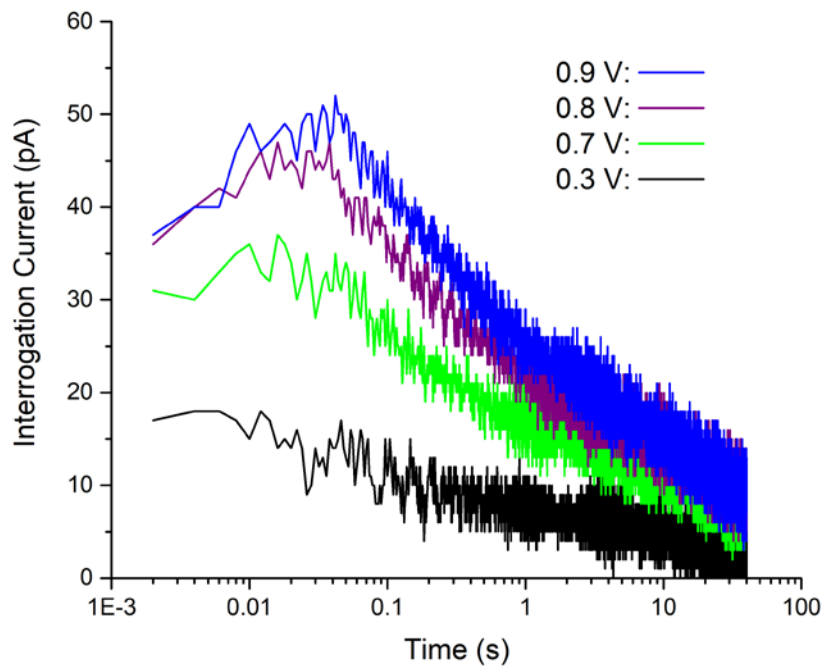


Figure S9. Surface interrogations of the hematite electrode with illumination restricted to visible light (>405 nm).

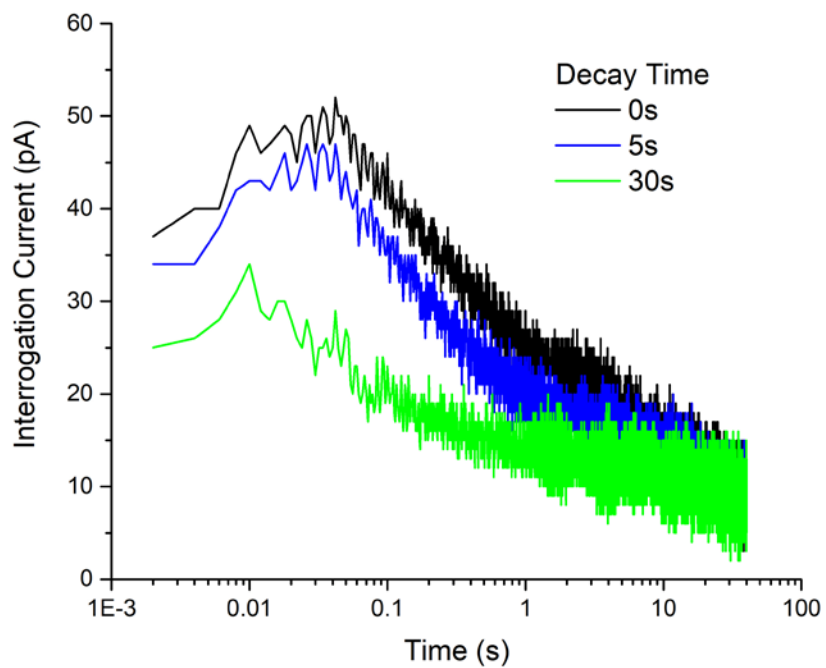


Figure S10. Delayed surface interrogations showing the decay of intermediates formed under visible illumination.

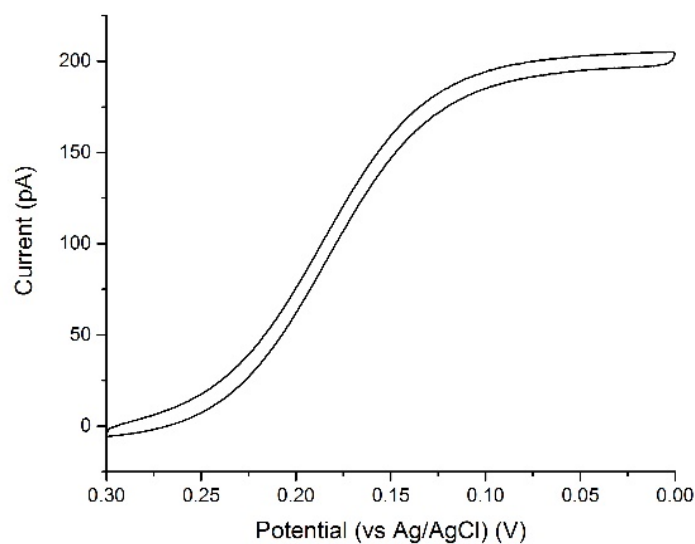


Figure S11. CV of a 4 μm carbon disk electrode in a borate buffer solution (pH = 9.4) containing 50 μM $\text{K}_3[\text{Fe}(\text{CN})_6]$.

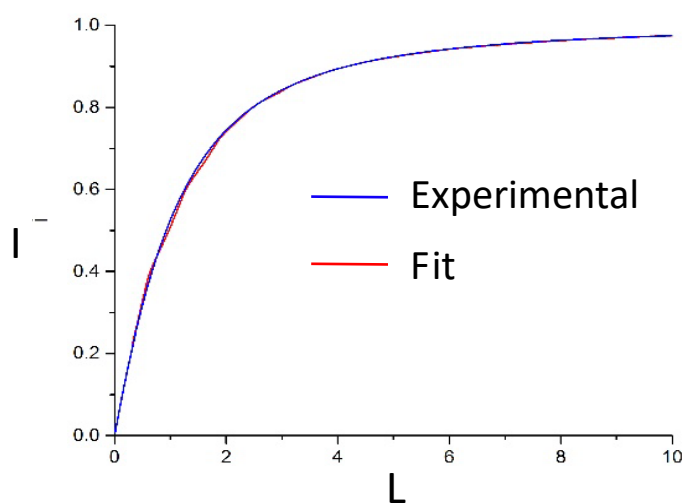


Figure S12. A experimental negative feedback approach curve to hematite and the fit to numerical models from reference 24 used to characterize the tip geometry for simulation of SI-SECM transients. This approach was performed with a 4 μm radius carbon disk electrode in a borate buffer solution (pH = 9.4) containing 50 μM $\text{K}_3[\text{Fe}(\text{CN})_6]$.

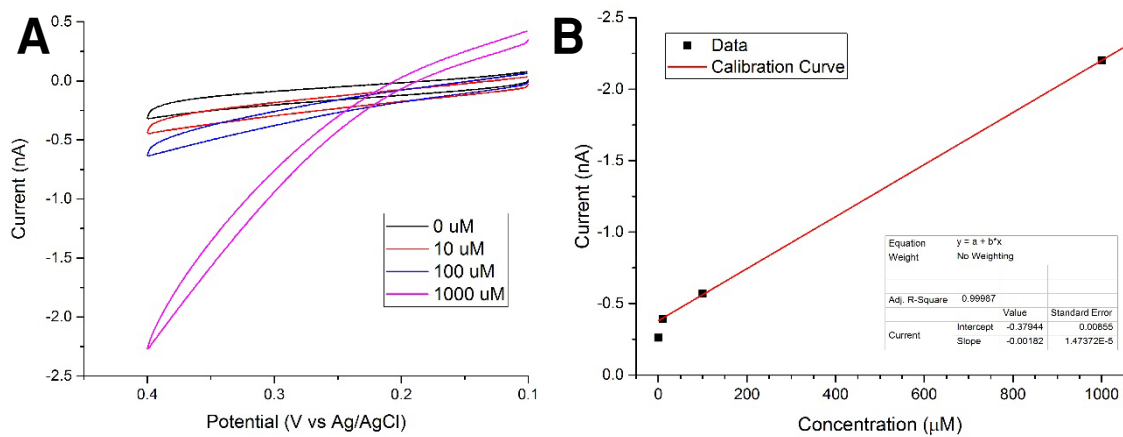


Figure S13. (A) Cyclic voltammograms of a Pt UME in an aqueous borate buffer (pH=9.4) with differing concentrations of H₂O₂. (B) The calibration curve

References

- (1) Simpson, B. H.; Rodríguez-López, J. *Electrochim. Acta* **2015**, *179*, 74-83.
- (2) Cornut, R.; Lefrou, C. J. *Electroanal. Chem.* **2007**, *608*, 59-66.